Copyright Warning & Restrictions

The copyright law of the United States (Title 17, United States Code) governs the making of photocopies or other reproductions of copyrighted material.

Under certain conditions specified in the law, libraries and archives are authorized to furnish a photocopy or other reproduction. One of these specified conditions is that the photocopy or reproduction is not to be "used for any purpose other than private study, scholarship, or research." If a, user makes a request for, or later uses, a photocopy or reproduction for purposes in excess of "fair use" that user may be liable for copyright infringement,

This institution reserves the right to refuse to accept a copying order if, in its judgment, fulfillment of the order would involve violation of copyright law.

Please Note: The author retains the copyright while the New Jersey Institute of Technology reserves the right to distribute this thesis or dissertation

Printing note: If you do not wish to print this page, then select "Pages from: first page # to: last page #" on the print dialog screen

NJIT
New Jersey's Science & Technology University

The Van Houten library has removed some of the personal information and all signatures from the approval page and biographical sketches of theses and dissertations in order to protect the identity of NJIT graduates and faculty.

ABSTRACT

TREATED HfO_2 BASED RRAM DEVICES WITH Ru, TaN, TiN AS TOP ELECTRODE FOR IN-MEMORY COMPUTING HARDWARE

by
Yuvraj Dineshkumar Patel

The scalability and power efficiency of the conventional CMOS technology is steadily coming to a halt due to increasing problems and challenges in fabrication technology. Many non-volatile memory devices have emerged recently to meet the scaling challenges. Memory devices such as RRAMs or ReRAM (Resistive Random-Access Memory) have proved to be a promising candidate for analog in memory computing applications related to inference and learning in artificial intelligence. A RRAM cell has a MIM (Metal insulator metal) structure that exhibits reversible resistive switching on application of positive or negative voltage. But detailed studies on the power consumption, repeatability and retention of during multi-level operation have not been undertaken previously.

Transition metal oxide-based RRAMs, using HfO_2, executes change in resistance (switching behavior) via electrochemical migration of oxygen vacancies. This thesis investigates the role of extra oxygen vacancies, introduced by plasma exposure (treated), in HfO_2 to reduce the power consumption of RRAM. In addition to oxygen vacancy rich HfO_2, various top metal electrodes including Ruthenium (Ru) are explored to enhance the switching behavior and power consumption. Use of Ru as a top metal reduced the switching energy of the treated HfO_2 RRAM device.

TREATED HfO_2 BASED RRAM DEVICES WITH Ru, TaN, TiN AS TOP ELECTRODE FOR IN-MEMORY COMPUTING HARDWARE

by
Yuvraj Dineshkumar Patel

A Thesis
Submitted to the Faculty of
New Jersey Institute of Technology
in Partial Fulfillment of the Requirements for the Degree of
Master of Science in Computer Engineering

Helen and John C. Hartmann Department of
Electrical and Computer Engineering

December 2020

Blank Page

APPROVAL PAGE

TREATED HfO_2 BASED RRAM DEVICES WITH Ru, TaN, TiN AS TOP ELECTRODE FOR IN-MEMORY COMPUTING HARDWARE

Yuvraj Dineshkumar Patel

Dr. Durgamadhab Misra, Dissertation Advisor | Date

Professor of Electrical and Computer Engineering, NJIT

Dr. Leonid Tsybeskov, Committee Member | Date

Distinguished Professor and Chair of Electrical and Computer Engineering, NJIT

Dr. Marek Sosnowski, Committee Member | Date

Professor of Electrical and Computer Engineering, NJIT

Blank Page

BIOGRAPHICAL SKETCH

Author: Yuvraj Dineshkumar Patel

Degree: Master of Science

Date: December 2020

Undergraduate and Graduate Education:

- Master of Science in Computer Engineering,
  New Jersey Institute of Technology, Newark, NJ, 2020

- Bachelor of Science in Computer Engineering,
  New Jersey Institute of Technology, Newark, NJ, 2019

Major: Computer Engineering

Dedicated to my teachers, parents and friends who inspired and motivated me towards my ambitions.

ACKNOWLEDGMENT

I would first like to owe a deep sense of gratitude to Dr. Durga Misra, Department of Engineering, New Jersey Institute of Technology, Newark, New Jersey for his keen interest in me at every stage of my research. While endlessly steering me into an appropriate direction when needed, he always permitted this research paper to be my own work. Thank you for tolerantly supporting me to improve in my weaker areas and recognizing my research strengths. I cannot suitably determine how appreciative I am to you. Without the advice and the constant help this disquisition would have been infeasible.

It is a genuine pleasure to express my deep sense of gratitude and thanks to my former mentor and role model, Dr. Bipin Rajendran, Reader in Engineering, King's College London, United Kingdom who introduced me to Neuromorphic computing and RRAMs. He guided me through my undergraduate education and shared the excitement of a year of research. Dr. Bipin's unwavering energy for research and personal generosity kept me constantly committed with my research which facilitated my time at NJIT.

I am grateful to my colleagues at Helmholtz Zentrum Berlin. During the Germany Research I learnt a great deal on fabrication and characterization of RRAMs. I equally appreciate Dr. Catherine Dubourdieu, Dr. Veeresh Deshpande, and Florian Maudet for all the informative talks and knowledge.

My gratitude extends to the faculty and staff of the Electrical and Computer Engineering department at NJIT who a joy has been to work with. I would also like to thank Nandakumar, Barsha and Anakha for all the assistance that was provided all along the line.

Above ground, I am beholden to my family, whose help and guidance are always with me. I would particularly like to thank my parents, whose value to me only raises with age. Thank you to my friends, professors, and classmates in education both past and present who have been with me through thick and thin during this marvelous adventure in completing my Master's Degree; I will never forget your willingness to believe in me, to question me, to encourage me, and to help me to achieve my dreams. I will forever remember how you are the reason that has made me the educator that I am today.

TABLE OF CONTENTS

Chapter **Page**

1 INTRODUCTION…......................................……………..………………………… 1

1.1 Background …......................................……………..………………………….... 1

1.2 RRAM Devices and Applications…………………………………………… 3

1.3 Types of RRAMs………………………………………………………… 5

1.3.1 Ferroelectric RAM (FRAM)..………………………………………... 5

1.3.2 Magnetoresistive RAM (MRAM)…………………………………….. 6

1.3.3 Phase Change Memory ………...……..………………………………… 7

1.3.4 Conductive Bridge RAM (CBRAM)...……………………………….. 8

1.3.5 Oxide Based RAM (OxRAM)...………………………………………… 9

1.4 Working Principle of Basic RRAM …………………………………………… 10

1.5 Motivation for The Thesis ………...…………………………….………… 12

1.6 Thesis Organization………………………………………………………. 12

2 CURRENT STATUS OF RRAM DEVICES WITH TRANSITION METAL DIELECTRIC…………………………………………………………………. 14

2.1 Detailed Working Principle of Transition Metal Oxide RRAM………………. 14

2.1.1 Advantages of HfO_x over HfO_2 ………………………..…………….. 16

2.2 Hafnium Based RRAM Devices.......... 17

2.2.1 Oxygen Variances Management.......... 17

2.3 Materials and Processing for Power Reduction 19

2.3.1 TiN as Top Electrode 19

2.3.2 Ti as Top Electrode.......... 20

2.3.3 Ru as Top Electrode 20

2.3.4 TaN as Top Electrode 21

2.3.5 HfO_2 as Switching Dielectric.......... 21

2.3.6 Plasma Treatment.......... 22

2.4 Top and Bottom Electrode Selection.......... 23

2.4.1 Barrier Height.......... 23

2.4.2 Effects of Change in Barrier Height in HfO_x and HfO_2.......... 24

2.5 Summary.......... 24

3 EXPERIMENTAL DETAILS.......... 26

3.1 Deposition Techniques.......... 26

3.2 Structure of The Devices.......... 27

3.3 Electrical Characterization of The Devices 28

3.4 Principle of IV Characteristics.......... 30

3.5 Summary………………………………………………………………………. 32

4 RESULTS OF TREATED DEVICES TO ENHANCE OXYGEN VACANCIES…………………………………………..…………………….. 33

4.1 TiN Devices…...……………………………………………………………... 33

4.2 Ru Devices……………………………………………………………………... 35

4.3 TaN Devices…………………………………………………………………. 36

4.4 Summary…………………………………………………………………….. 38

5 COMPARISION OF DIFFERENT METALS……………………………………... 39

5.1 Comparison Between Ru and TaN, TiN Devices……………………….……... 39

5.2 Switching Characteristics……………………………………………………. 40

5.3 Resistance Distribution …………………..……………………………………… 41

5.3.1 Resistance Distribution in Ru Devices..………………………………..... 41

5.3.2 Resistance Distribution in TiN Devices …...…………….…..……..……… 42

5.3.2 Resistance Distribution in TaN Devices …..…………….…..……..……… 43

5.4 Summary……………………………………………………………………. 44

6 CONCLUSION AND FUTURE WORKS………………………………………… 45

6.1 Future Work 46

REFERENCES …….………………………………………………………………. 47

LIST OF TABLES

Table **Page**

1.1 Shows Different Configuration of RRAM Devices with Unipolar and Bipolar Switching Characteristics. ………..…………….…….…………………………………. 11

2.1 Table with Formation Energy and Cohesion Energy of Vacancies with Different Charge is Shown. …………………………………………………………….…. 19

LIST OF FIGURES

Figure		Page
1.1	The graph of technology node vs transistor manufacturing cost…………………	1
1.2	SoC Design comparison vs manufacturing year………………………………….	2
1.3	(a) RRAM structure (b) Unipolar switching (c) Bipolar switching………………	3
1.4	Periodic table with oxide and electrode details used for RRAMs………………..	4
1.5	Evaluation of RRAM devices…………………………………………………….	5
1.6	Hysteresis curves of RRAM devices……………………………………………..	6
1.7	MRAM structure…………………………………………………………………	7
1.8	PCM device structure and SET and RESET graph………………………………	8
1.9	Device structure of CBRAM……………………………………………………..	9
1.10	(a) Unipolar switching, I-V characteristics (b) Bipolar switching I-V characteristics…………………………………………………………………….	12
2.1	Switching mechanism in RRAM…………………………………………………	16
2.2	(a) The electron flow mechanism in leaky HfO_x (b) The electron flow mechanism in stoichiometric HfO_2……………………………………………	17
3.1	Structure of the devices that are used for the thesis study………………………..	27
3.2	Picture of Keysight B1500 semiconductor……………………………………….	28
3.3	The remote-sense and switch unit connection to the B1500A	29
3.4	The forming process, SET-RESET process and the compliance current in the I-V characteristic of a general oxide-based RRAM………………………………..	30

4.1 I-V characteristics of the devices with TiN as top electrode…………………….. 34

4.2 I-V characteristics of the devices with Ru as top electrode……………………… 35

4.3 I-V characteristics of the devices with TaN as top electrode……………………. 37

5.1 Cumulative Resistance distribution of the devices with Ru as top electrode……. 41

5.2 Conducting Filament formation as a function of compliance current…………… 42

5.3 Cumulative Resistance distribution of the devices with TiN as top electrode…... 42

5.4 Cumulative Resistance distribution of the devices with TaN as top electrode….. 43

CHAPTER 1

INTRODUCTION

1.1 Background

Semiconductor has played a vital role in the technology world, especially semiconductor memory technology has implemented a wide variety of applications for users. In comparison, for mass production and high performance, continuous scaling of semiconductor technology has allowed high density integration. Non-volatile NAND Flash memory represents a significant portion of the industry. Scaling it down further from 20 nm technology nodes has not drastically increased the performance. However, the scaling has increased the fabrication cost. The scaling down of the technology node has not significantly reduced the scaling cost per transistor in recent nodes, as shown in figure 1.1 and figure 1.2 [1].

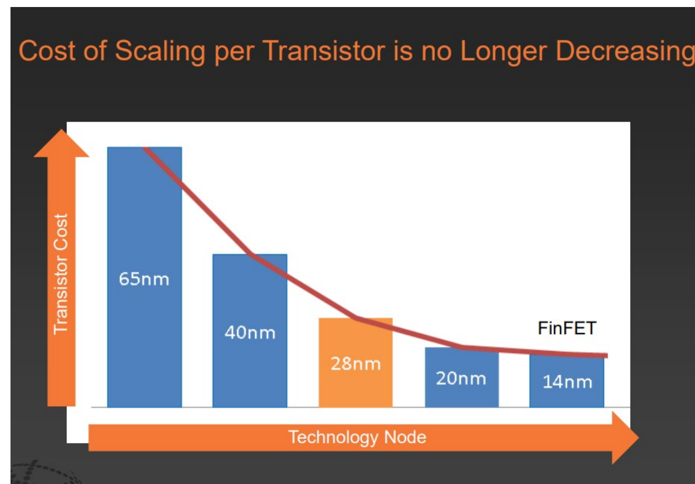

Figure 1.1 The graph of technology node in nm vs transistor manufacturing cost is shown.
Source: [1]

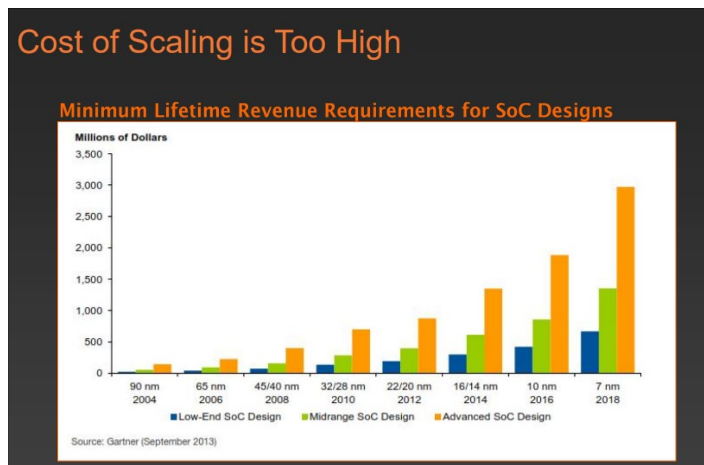

Figure 1.2 Three types of SoC design is compared in the graph with the manufacturing year and technology node vs the cost in millions of dollars.
Source: [1]

Different types of memory systems have been suggested as an alternative approach to the existing memory systems, which can be combined with the existing CMOS technology for improved performance, lowered fabrication costs, and therefore, lower the overall power requirement. Resistive Random Access Memory (ReRAM or RRAM) has more benefits than the current emerging technology, but it stands out as a serious contender for NAND Flash memory. Furthermore, the evolution of in-memory computing and artificial intelligence hardware requires more innovative RRAM devices.

RRAM technology has proved itself in many aspects of semiconductor technologies, like high speed switching, high storage density, enhanced scalability, and multilevel storage capacity. Although such characteristics such as endurance, retention and controllability of switching characteristics are being investigated further [2] to integrate into standard CMOS nodes.

1.2 RRAM Devices and Applications

The RRAM technology can be integrated into many areas such as Neuromorphic computing, AI, Nano storage memory [3], Non-volatile logic and security applications etc. Ironically, more than 50 years ago [4-6], the fact that insulators can have a change of resistance while adding electrical filings was discovered. But after 2004, when Samsung presented a paper at the Electron Device Meeting, the industry started taking an interest in resistive switching memory. Fig. 1.3 shows the evaluation and market share of RRAM from 1962 to 2017.

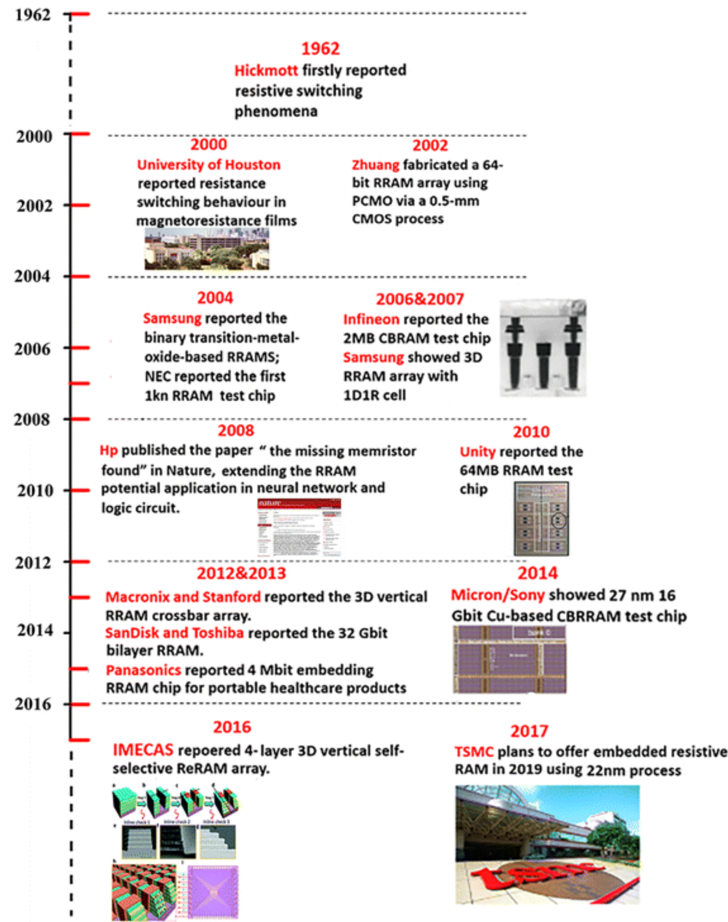

Figure 1.3 The evaluation of the RRAM devices.
Source: [7]

The RRAM's common structure consists of an insulator sandwich between two metals, in the shape of a metal-insulator-metal capacitor. The resistance of the insulator that serves as the switching layer is modified when an electric field is applied to the top and bottom metal electrodes, as shown in figure 1.4 (a). The device switches between a high resistance state (HRS) to a low resistance state (LRS). This is possible because of the formation of a conducting filament between the electrodes. In some cases, a unipolar potential can switch the device from HRS to LRS and LRS to HRS (figure. 1.4b). In other instances when a reverse potential is applied the conducting filament ruptures and the devices returns back to HRS (figure. 1.4c). Depending on the structural composition of the switching layer of the RRAM, the choice of top metal and the bottom electrode the switching characteristics will differ, as shown by figure 1.4b and figure. 1.4c.

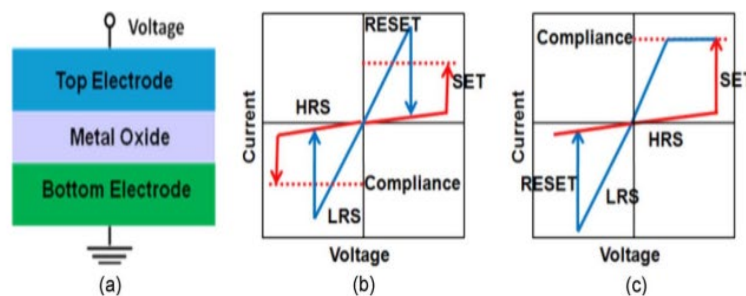

Figure 1.4 (a) Schematic of MIM structure for metal-oxide, and schematic of metal-oxide memory’s I-V curves, showing two modes of operation: (b) unipolar and (c) bipolar.
Source: [8]

Various combination of insulating materials and top and bottom electrode metals determines the formation of the RRAM device. The elements in the periodic table that

exhibit bistable resistance switching materials are shown in yellow in Fig. 1.5 and the metal that can be used for electrode are shown in blue [8][9].

Figure 1.5 Periodic table with elements able to exhibit bistable resistance switching are shown in yellow, and the metal that can be used for electrode are shown in blue.
Source: [8][9]

1.3 Types of RRAMs

RRAMs exhibits switching characteristics by change in resistance. However, change in resistance can be achieved using various techniques or materials. In this section a few different devices are discussed that have unique way to store memory and have various characteristics.

1.3.1 Ferroelectric RAM (FRAM)

In 1987, FRAM (Ferroelectric Random Access Memory) has been introduced for the first time and reported low power consumption and high endurance [10]**.** FRAM is made of a ferroelectric capacitor, commonly PZT(Pb(Zr,Ti)O3), which is responsible for switching characteristics. The resistance change happens as a result of the change in polarization

introduced by electric fields. Hysteresis behavior is shown after electric field application, as can be seen in figure. 1.6 [11]. FRAM is indeed not readily scalable, restricting its usage to limited storage space devices. Usually, PZT and the electrode material, which is mainly inert material, typically create scaling process difficult [12].

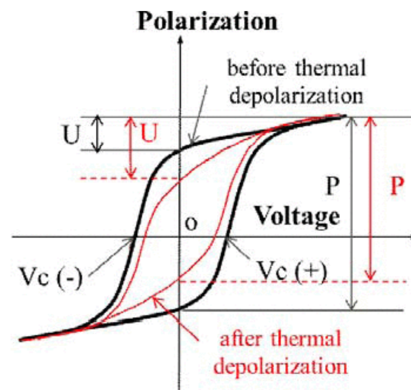

Figure 1.6 Polarization-voltage (p-v) hysteresis curves are shown. Black line and red line show the p-v hysteresis before and after thermal depolarizations.
Source: [13]

1.3.2 Magnetoresistive RAM (MRAM)

MRAM stands for Magnetoresistive Random Access Memory, which uses two key electron characteristics, namely 'spin and charge' to store the data. MRAM is classified into devices that use magnetic moment (spin) and charge and are referred to as spin electronics devices.

The structure of the MRAM device, shown in figure 1.7, demonstrates a layer stack in between the electrodes in the form of a Magnetic tunnel junction (MTJs). MTJ facilitates electron transport by the phenomenon of tunneling. Under the top electrode, the first layer is called the free layer, where the magnetic orientation is programmable. The bottom-most layer is called the pinning layer and the reference layer is called on top of that. The pinned layer and the free layer are separated by a thin insulator that enables electron tunneling. At the time

of fabrication, the magnetic spin on the pinned layer is fixed. The pinned layer contributes to the MRAM in reading and writing. To form the anti-ferromagnet structure, the pinned layer has two sublayers that are separated by Ruthenium [14][15].

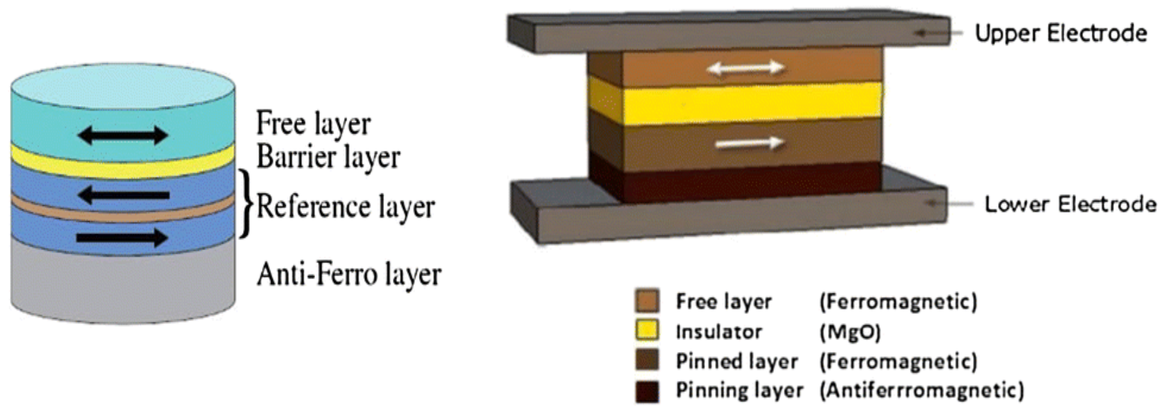

Figure 1.7 MRAM structure is shown in the figure, with different layers and their names.

The newer memory called Spin Transfer Torque-MRAM(STT-MRAM) has enhanced the speed, power consumption, better scalability and endurance of MRAM performance. Scalability for this technology, though still remains a bottleneck [16].

1.3.3 Phase Change Memory

PCM stands for Phase Change Memory, which follows a similar concept to CDs and DVDs for memory storage. PCM is known to be one of the most advanced RRAM innovations to come [17]. PCM defines two stages of transition in resistivity: polycrystalline and amorphous. Low resistivity refers to the polycrystalline phase and high resistivity applies to the amorphous phase. PCM employs chalcogenides as they have shown phase shift capabilities.

As shown in the figure 1.8, changes in phase material activate the resistance change and thus control the PCM memory cell's conductivity based on an applied voltage. During fabrication of PCM, the crystallized phase (ordered) is set. The material must be heated above its melting point to achieve an amorphous phase from the crystalline phase. After the heat treatment it settles rapidly to a disordered state. The material must be heated below the melting point to obtain the crystalline phase back from the amorphous phase (disordered). There would be high resistance to the amorphous phase and low resistance to the crystalline phase. Considering its high speed, endurance and extremely high retention capacity, PCM memory has the potential to replace existing DRAM technologies. In recent years, with current memory technologies, PCM has also started to come to market as hybrid memory. Intel also released the data memory Optane, which uses PCM as the latest hybrid memory technology [18].

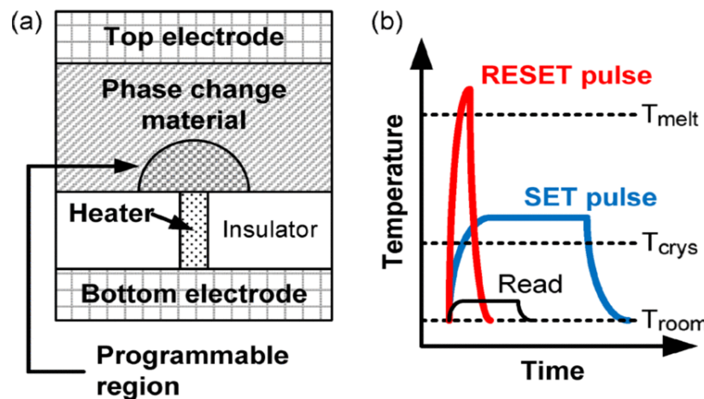

Figure 1.8 (a) Device structure of the PCM with the switching dielectric and **(b)** The SET-RESET pulse graph is shown.
Source: [17]

1.3.4 Conductive Bridge RAM (CBRAM)

CBRAM is known as a conductive Bridge RAM or programmable metallization cell. Due to the forming and breaking of conductive filament (CF) in solid electrolyte, resistive switching in CBRAM occurs. Filament formation and breakage are known to be due to the movement of metal ions [19][20].

We can see that CBRAM consists of three layers, the top electrode, the solid electrolyte and the bottom electrode, as shown in the figure 1.9. Usually, the top electrode or active layer is made of Ag or Cu, the solid electrolyte may be made of chalcogenide material, and usually the bottom layer or inert layer is made of inert material such as Pt or W.

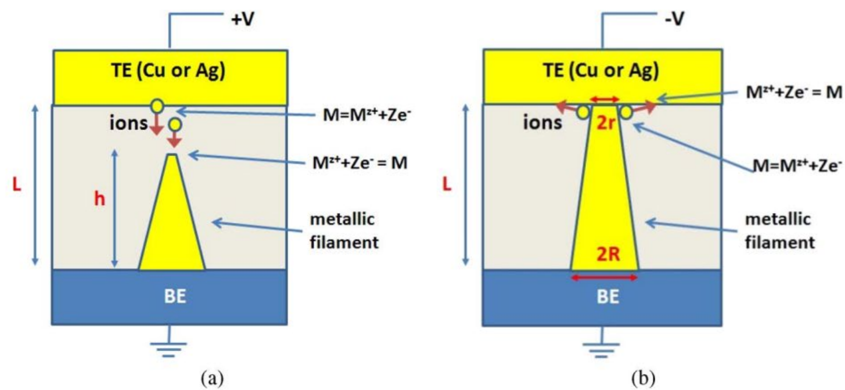

Figure 1.9 Device structure of CBRAM is shown in the figure with (a) HRS (b) LRS.

The set process Fig. 1.9(a) occurs when a device is placed under a positive electric field, the metal ions from the top electrode forms CF and that filament is ruptured from the top metal when a negative electric field is applied, thus reset occurs. In comparison, CBRAM exhibits low energy consumption, high endurance and good scalability.

1.3.5 Oxide-based RAM (OxRAM)

OxRAM stands for oxide-based RAM. MIM is the RRAM unit structure (metal-insulator-metal). The insulator is resistive oxide that is normally sandwiched between two metal electrodes. The oxide resistance is altered by the application of electric field. Low resistance state (LRS) is obtained when a positive electric field is applied, while high resistance state (HRS) is obtained when a negative electric field is applied. OxRAM's switching mechanism is based on the oxide used for fabrication. There are two types of classification: electrochemical metallization effect and the oxygen vacancy migration effect [7]. Electrochemical metallization includes a conductive filament formation of metal ions in the insulator lattice after the application of a positive electric field (LRS) and the rupture of the conductive filament occurs after the application of a negative electric field (HRS). Oxygen vacancies, though, are responsible for the formation of the conductive filament in the later type of OxRAM. Since OxRAM with an oxygen migration effect is the topic of research of this study, the next section discusses the thorough understanding of the operating mechanism.

1.4 Working Principle of Basic RRAM

As discussed in the above sections, the basic mechanism of RRAM consists of a change in the resistance state. The transition from the state of high resistance (HRS) to the state of low resistance (LRS) is called the SET process, while the change from LRS to HRS is called the RESET process. The initial voltage that the device switches is called forming voltage in the SET process, so that the voltage to which the device switches is marginally greater than the set voltage. This process is called conductive filament formation. A compliance current is set to reduce the current on both the SET and RESET processes in order to control the growth of

the filament and prevent permanent dielectric breakdown. However, until the electric field is applied the unit remains in either LRS or HRS state, which illustrates the non-volatile nature of the RRAM. Like conventional CMOS technology, reading the SET or RESET state ('1' or '0') involves the use of very limited voltage amounts. The switching system is primarily categorized into two types: Unipolar and Bipolar switching, depending on the SET and RESET phase categorization. The unipolar switching, as shown in the figure 1.10(a), does not depend on the polarity of the electric field applied across the device, but on the magnitude of the compliance current. However, if the bipolar switching occurs when the polarity is switched (positive and negative voltage), then it is called bipolar switching. In bipolar switching, however, the principle is opposite to unipolar switching, as shown in figure 1.10(b) where at the positive voltage the SET process takes place and at the negative voltage the RESET process takes place. Table 1.1 displays some of the device structures that have shown the mechanism of Unipolar and Bipolar switching [21][22].

Table 1.1 Shows Different Configuration of RRAM Devices with Unipolar and Bipolar Switching Characteristics

Unipolar	Bipolar
Pt/NiO/Pt [7]	Pt/NiO/$SrRuO_3$ [54]
Pt/TiO_2/Pt [8]	Pt/TiO_2/TiN [55]
Pt/ZnO/Pt [18]	TiN/ZnO/Pt [56]
Pt/ZrO_2/Pt [57]	Ti/ZrO_2/Pt [57]
Pt/HfO_2/Pt [58]	TiN/HfO_2/Pt [59]
Pt/Al_2O_3/Ru [60]	Ti/Al_2O_3/Pt [61]

Source: [8]

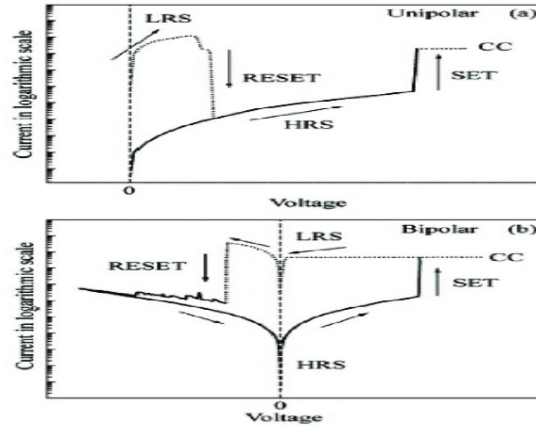

Figure 1.10 (a) Unipolar switching I-V characteristics (b) Bipolar switching I-V characteristics.
Source: [23]

1.5 Motivation for The Thesis

Low power consumption, speed improvement, high endurance and retention rate can make the RRAMs very beneficial to the current silicon industry. Even though as there is a lot of research going on to come up with a reliable RRAM technology, there is still no prominent players in the industry. On the brighter side, in combination with conventional CMOS technology, several enterprises have already begun developing RRAM products. In addition, the aim of this thesis is to provide support to the current research of RRAM in terms of switching power reduction. This work is motivated to give valuable knowledge for further research by providing useful information on transition metal-oxide RRAM that exhibits very low power switching characteristics.

1.6 Thesis Organization

Chapter 1 describes a high-level knowledge of the Silicon market to emerging cutting edge techniques for memory cells, comprising the background details and general information about the RRAMs.

Chapter 2 introduces Transition metal-oxide RRAM, and provides comprehensive knowledge about the operating mechanism, and structural details. In particular, the devices covered in this research paper are illustrated with details of the materials used to fabricate the devices and their effects on the switching mechanisms.

Chapter 3 outlines the experimental details used in this thesis. Various deposition techniques used to fabricate the device, the structure of the device, and the measurements techniques are explained.

Chapter 4 represented the results of the experiments. It includes plots on the top layer of the characteristics of the device with various metals.

Chapter 5 reflects a comparison of the findings given in Chapter 4 as per the use of various top electrodes. Using resistance plots, it compares various metals and possible multi-level states.

Chapter 6 summarizes and concludes as well as the future analysis that can be performed in the study on the devices presented.

CHAPTER 2

CURRENT STATUS OF RRAM DEVICES WITH TRANSITION METAL DIELECTRIC

The dielectric layer plays an important role for the RRAM switching. Recently, many transition metal oxides such as HfO_2-based RRAM devices are reported to exhibit nonvolatile data storage potential. HfO_2 is extensively studied for the RRAM application. However, stoichiometric HfO_2 is not suitable because of lack of enough oxygen vacancies and requires high forming voltage that leads to higher power consumption. Therefore, different HfO_2 based dielectric materials are investigated to improve the performance of RRAM devices. In the following sections we discuss the working principle and various methods to control the oxygen vacancy concentration in transition metal oxides.

2.1 Detailed Working Principle of Transition Metal Oxide RRAM

Transitional metal oxide RRAM have two operation mechanism as discussed before. In this section OxRAM with oxygen migration will be discussed. The mechanism of switching of the RRAM to execute reversible LRS ('0') and HRS ('1'), involves initialization of forming process. As mentioned in the above section, the mechanism involves migration of oxygen ions, O^{2-} and thereby generating oxygen vacancies (V_o^{+2}). The forming process initializes a conducting path or a conducting filament when a fresh sample is placed under an electric field. The voltage is typically higher than the set voltage. Once higher voltage is applied, soft dielectric breakdown occurs, and as shown in the Fig. 2.1. The oxygen atoms present in the dielectric material starts moving towards anode in form of oxygen ions (O^{2-}) and leaving

behind oxygen vacancies (V_o^{+2}). The oxygen vacancies form the conducting filament from cathode and anode [24]. The oxygen ions at the anode interface forms an interfacial oxide layer by reacting with the top metal at anode or getting discharge as non-lattice oxygen (if the top interface is inert material), making the anode interface oxygen rich. The electron flow is established in the CF by the oxygen vacancies, and hence a LRS is observed. Multiple connections are formed with the top metal instead of a single connection, moreover, the number of connections is controlled by the compliance current which prevents dielectric breakdown. However, two types of RESET process are possible depending on the material structure. In the unipolar switching after application of higher current, the oxygen ions migrate back to CF and combines with oxygen vacancies, because of Joule heating current. In the bipolar switching inverse electric field must be applied for the oxygen ions present in the interfacial layer to overcome the diffusion barrier and migrate towards the oxygen vacancies. Once the oxygen ions combine with the oxygen vacancies, the conductive path is ruptured, and the sample returns the HRS.

During the SET process the ruptured CF is repaired. Therefore, the SET voltage is lower than the initial forming voltage. The process of SET and RESET is repeatable until the permanent dielectric breakdown occurs in which the oxygens ions are not able to overcome the diffusion barrier and there is a permanent formation of CF [24][25].

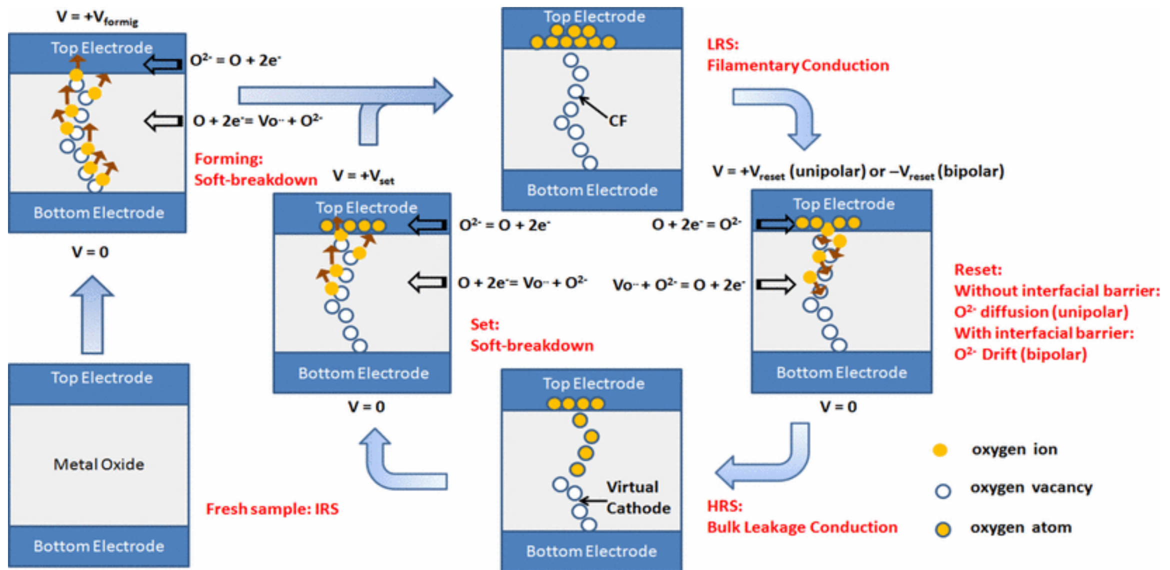

Figure 2.1 Switching mechanism in RRAM with oxygen migration is shown with markers of oxygen ions, oxygen vacancy and oxygen atom. A complete SET-RESET process is shown with forming process.
Source: [8]

2.1.1 Advantages of HfO_x over HfO_2

The switching characteristics depends both the switching dielectric and top/bottom electrode. In this thesis, devices with Hafnium oxide-based dielectric are studied. However, in previous studies a stoichiometric HfO_2 dielectric layer as shown higher amount of power requirement for switching. Stoichiometric HfO_2 has reduced amount of free oxygen vacancies, and because of that higher CC is required to knockout more oxygen vacancies and form the conductive filament [26]. As a result, there is large overshoot of current in the forming process and a CF with larger diameter is formed. Also, due to high CC the knocked-out oxygen ion forms permanent bond the top electrode making it hard to break the CF and perform RESET. The non-stoichiometric HfO_x has a large number of oxygen vacancies, introduced during the fabrication process

or because of the selection of top/bottom electrode. Due to presence of oxygen vacancies, a rather soft dielectric breakdown occurs with lower CC as shown in the figure 2.2. There is a smaller current overshoot leading to formation of CF in controlled manner [28] [27].

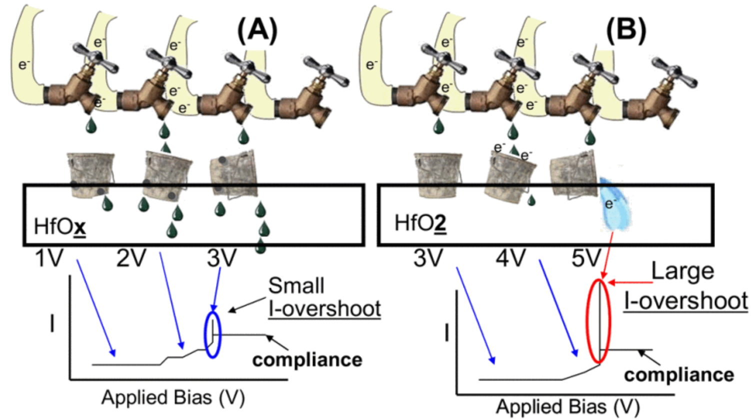

Figure 2.2 (a)The electron flow mechanism in leaky HfO_x is shown with the CC vs applied voltage graph (b) The electron flow mechanism in stochiometric HfO_2 is shown with the CC vs applied voltage graph.
Source: [26]

2.2 Hafnium Based RRAM Devices

As present HfO_2 is used as a gate dielectric in standard CMOS technology. Therefore, use of HfO_2 as a switching dielectric in RRAM devices is desirable because of it compatibility for integration in CMOS technology [29]. In this study, hafnium-based RRAMs are studied that will be explored further in depth with separate selections of top electrodes.

2.2.1 Oxygen Vacancies Management

Oxygen vacancies play a significant role in CF formation and therefore control the process of switching. The oxygen vacancies are uniformly distributed in the HfOx over

the thickness of the layer. However, depending on the top and bottom electrodes, the concentration of the vacancies can be more or less towards the top or bottom electrode interface. Details regarding the impact of top and the bottom electrodes are discussed in the subsequent section of this chapter. Reactive metal electrodes such as Ti or TiN scavenge oxygen ions form the dielectric and form interfacial layers of TiOx or TiON respectively. After the application of electric potential across the device, interfacial layers are formed. The oxygen ions, however, stay in oxide depending on the top metal or oxidize with the top metal. Studies have shown that reactive metals such as Ti, TiN, relative to inert metal electrodes such as Pt, exhibit less forming and set voltages.

The switching mechanism is controlled by oxygen vacancies with different charges. In a study conducted by Chung et al [30] it is stated that Hafnium oxide layer contains oxygen vacancies with charge states: 0, +1 and +2. Oxygen vacancies with charge states 0 and +1 have negative cohesive energy and because of that they tend to cluster and form the conducting filament [30]. Table 1 shows the cohesion and formation energy for the vacancies with different charge states. The study also states a forming model which states that knocked out oxygen ion passed through the metal/oxide interface and generates vacancies with charge state +2 which then traps electrons from bottom electrode and forms neutral oxygen vacancies with 0 charge. The neutral vacancies cluster around to form CF, however the study suggest strong presence of vacancies with charge +1 in the CF as the migration barrier height of the neutral oxygen vacancy in HfOx is much higher that the operating voltage.

Table 2 Table with Formation Energy and Cohesion Energy of Vacancies with Different Charge is shown

	V_O^0	V_O^+	V_O^{++}
Formation Energy (eV)	> 4eV	< 0 eV	< -4eV
Cohesion Energy	Negative	Negative	Positive

Source: [30]

2.3 Materials and Processing for Power Reduction

There is a great deal of research going on to find the appropriate material configuration for RRAMs to reduce power. The power demand for the device has been improved by various configurations, such as the inclusion of a buffer layer in the device structure, before or after the switching dielectric layer. In a recent study [31], the Al_2O_3 buffer layer in the RRAM based on HfO_2 induced a significant reduction in power relative to standard HfO_2 RRAM. Since Al_2O_3 has lower activation energy (1.8eV) than HfO_2 (4.6 eV) oxygen vacancies are produced at a higher rate in the Al_2O_3 layer. When this buffer layer is introduced between the top electrode and the dielectric switching power is significantly reduced as compared to when this buffer later is introduced between the bottom electrode and the HfO_2. Therefore, distribution of oxygen vacancies in the dielectric is critical to switching power reduction in the RRAM devices.

2.3.1 TiN as Top Electrode

Titanium nitride is a less reactive towards oxygen then titanium (Ti). TiN is used as a buffer layer in addition to Ti for more control over CF formation in RRAMs with oxygen

migration-based switching. Previous studies have shown a tighter distribution of set and reset voltages with TiN used as buffer layer to the top electrode [32]. Upon application of an electric field to the device, oxygen scavenging layer of Ti attracts oxygen ions towards itself however, upon continuous cycles of set and reset this proves to be a side effect as the device keeps on getting degraded. But it is believed that addition of TiN buffer layer to the Ti layer controls this scavenging of oxygen in a controlled manner and regulates HRS and LRS to a tighter variation. The work function of Ti is around 4.3ev whereas of TiN is 4.5ev, which results in movements of electrons from Ti towards TiN.

2.3.2 Ti as Top Electrode

Titanium (Ti) is considered to be reactive to the oxygen [33] [34] and previous studies have shown that the Ti/HfO_2 interface has accounted for more oxygen vacancy in the dielectric layer. After being placed under an electric field, Ti in the RRAM reacts with the oxygen ions present in the oxide-electrode interface. The reaction results in TiOx and HfO2-x through the interface with the x variable. Oxygen ions, however, form a reactive Ti electrode compound and thus leave behind oxygen vacancies that assist in the formation of CF. A clustered structure forms the oxygen vacancies and thus creates a conducting path for the electrons to pass and set the device to LRS. Therefore, Ti as a top electrode tends to minimize set voltage, but by trapping much of the oxygen ions needed for the reset process, it also affects the reset process [35].

2.3.3 Ru as Top Electrode

Ruthenium (Ru) is an inert electrode used as a top metal electrode in the RRAM studied in this thesis. Ru is a transition metal with one electron in its outer most orbit. The work function of Ru is 4.7eV [36] with electrical resistivity of $\rho_{bulk} = 7.1$ µΩ.cm. Ru top metal electrode attracts more oxygen towards metal-dielectric interface, increasing the concentration of oxygen vacancies at the Ru/HfO_2 [37].

Ru metal as top electrode with HfO_2 have shown good reactivity towards oxygen present in the interface causing to increase in work function after the interfacial RuO_x oxide layer is formed. The oxidation of Ru leads to formation of more oxygen vacancies in the oxide layer and thereby contributing to the switching power reduction. [38]

2.3.4 TaN as Top Electrode

TaN exhibits bipolar switching characteristics as expressed in reference [39]. The research paper also claims that RRAM with TaN as top electrode shows quasi-ohmic current in its low resistance state and ohmic and space charge limited current in high resistance state. TaN shows similar properties to TiN top metal electrode, the switching mechanism of RRAM with TaN as top electrode involves formation of oxygen vacancies as a conductive path and rupturing of the conductive path by recombination of the oxygen ions [40].

TaN shows great reactivity toward oxygen and oxidizes to TaON because of oxygen scavenging property. The interfacial layer to the TaN (top metal electrode) and dielectric with form a non- uniform oxide layer which further changes the interface property and helps in the switching characteristics. [41]

2.3.5 HfO_2 as Switching Dielectric

Hafnium oxide is used commonly for transition metal oxide RRAM as a switching layer. It is mostly deposited using atomic layer deposition (ALD) technique for achieving thin-layer films with more control, uniformity and good interface. ALD deposited hafnium oxide films are very stochiometric with very a smaller number of defects. However, in oxygen vacancies-based switching RRAM, presence of more defects is necessary to avoid hard breakdown and ensure reversible switching [28][42]. To increase the number of defects in the hafnium oxide layer for lowering the power of forming voltage and set voltage, reactive layer of Ti, TiN or Ta are usually deposited as top electrodes which reacts with the knocked-out oxygen ions and produces extra oxygen vacancies. Moreover, other techniques to increase the defects in hafnium oxide like oxygen plasma treatment is explained in next section. [43].

The calculated activation energy for HfO_2 is 4.6eV [44], it is significant in formation and rupture of CF. Also, the grain boundaries present in the HfO_2 lattice account for the path of the soft-dielectric breakdown, that leads to formation of conductive path [45].

2.3.6 Plasma Treatment

Oxygen plasma treatment on hafnium oxide dielectric layer is performed for reduction in switching power. As explained in section 2.1, oxygen vacancies play major role in

switching mechanism. Extra oxygen vacancies formation in the dielectric layer can cause power reduction. The oxygen plasma treatment can increase number of defects in the HfO_2 layer [46], the layer is exposed to oxygen plasma for certain amount of time. This introduced defects (oxygens ions and oxygen vacancies), in the layer which further helps in CF formation and power reduction.

2.4 Top and Bottom Electrode Selection

Proper selection of top and bottom electrode metals is required for enhanced performance, endurance, retention rate and power reduction. Physical properties such as barrier height are highly responsible for switching mechanism in RRAM devices. The role of top electrode is superior as compared to bottom electrode in oxygen migration in RRAM since the reaction of top electrode is highly responsible for the CF formation. The bottom electrode is responsible for generating extra vacancies in the dielectric layer and providing electrons for conduction mechanism.

2.4.1 Barrier Height

Barrier height are resultant from difference in the energy barriers of the two material. In our case barrier height is observed at the interface of the metal and dielectric or oxide layer. This dielectric-metal interface barrier height is called Schottky barrier height. The exchange of electrons at the interface results in the barrier height, the estimation of the barrier height is done by calculating the difference of the work function of the materials. [47]. The barrier height is modulated by the reactivity of the top metal electrodes and the defects present in the dielectric layer.

The barrier height of the TiN/HfO_2 interface is lower than the barrier height of the TiN/SiO_2, according to previously conducted studies the barrier height of the HfO_2/TiN interface is calculated to be 1.6eV [48] [49]. The oxygen scavenging property of TiN is reasonable for lowering of the barrier height. Similarly, the barrier height of the TaN interface is found to be 1.08-1.68eV [50] considering the electron affinity of HfO_2 to be 2.08eV and work function of TaN to be 3.9-4.5eV. The barrier height of the Ru interface should be similar considering the similar work function of 4.7eV [37]. The oxygen plasma treatment of the HfO_2 changes the electron affinity and reduces the barrier even further. The Schottky barrier height changes after the filament formation depend on the LRS or HRS. When the CF is formed extra vacancies are generated (depending on the current flow) and that lowers the barrier height [30].

2.4.2 Effects of Change in Barrier Height in HfO_x and HfO_2

The barrier height is responsible for the amount of oxygen ions diffusion into the top metal electrode and formation of interfacial oxide layer that controls the growth of CF and therefore, is responsible for the switching power. Effect of lowering of barrier height is highly responsible for the reduction in the switching power requirement. Lower barrier causes more oxygen ions to react with the oxygen scavenging top electrode and thereby leaving less free oxygen ions to join back with oxygen vacancies which helps in required set and forming power.

2.5 Summary

To summarize, this chapter covered the reported recent literature of RRAM devices with transition metal oxides that exhibit switching characteristic using oxygen vacancies in the metal oxide. Detailed switching characteristics of RRAM was explained in first section, which includes the clustering of oxygen vacancies in the oxide layer to form CF on application of electric field across the top and the bottom electrode. It also states the advantages of non-stochiometric HfO_x over stochiometric HfO_2 due to presence of oxygen vacancies that help in reducing the set voltage and help the devices to switch at lower compliance current. Moreover, this chapter introduces to the hafnium-based RRAM and oxygen vacancies management which is the focus of the thesis. It also describes the selection of top and bottom electrode metals based on certain physical and chemical properties.

CHAPTER 3

EXPERIMENTAL DETAILS

This chapter covers the details of the structure of the devices that were studied in this thesis. Also, it contains the deposition techniques that were used to deposit the layers of the RRAM devices. Moreover, in the later section description of the tools used to characterize the devices is provided.

3.1 Deposition Techniques

The devices were fabricated at Tokyo Electron Limited (TEL) using different deposition techniques. 300 mm wafer was used to deposit the devices and then later diced in to 4 pieces for studying electrical characteristics. The structure of the devices is further explained in next section, the switching layer of HfO_2 is deposited using atomic layer deposition technique (ALD). The ALD process is carried out on TEL Trias^{+TM} platform with shower-head type 300mm reactor, Tetrakis (ethylmethylamido) hafnium was used as Hf precursor for HfO_2 deposition at 250°C deposition temperature and H_2O as co-reactant. The detailed HfO_2 deposition is discussed in, [28], [44], [51], [52]. However, developing novel idea of plasma treatment of oxide layer was introduced. HfO_2 was exposed to oxygen plasma to introduce defects into the layer which helps in the power reduction of the RRAM.

ALD technique was also used to deposit TiN for device with Ru as top electrode. Physical vapor deposition (PVD) techniques was used to deposit other top metal and bottom metal electrode. Moreover, ultra-high vacuum was used for all the deposition

techniques to avoid oxidation of the layer. MIM structures were analyzed using Titan aberration-corrected scanning transmission electron microscope (AC-STEM) at 300kV and was patterned using standard photolithography. Focused-ion beam (FIB) methods were used to develop the samples, electron beam was used to record the bright-field (BF) and high-angle annular dark field (HAADF) images.

3.2 Structure of The Devices

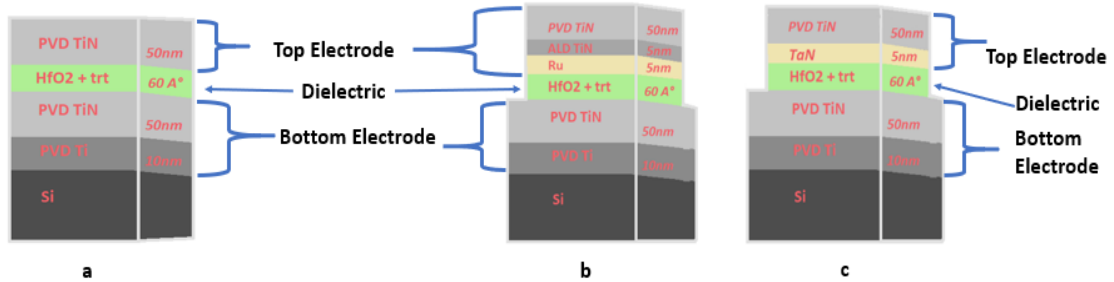

Figure 3.1 (a) Device structure of PVD Ti/PVD TiN/HfO_2/Ru/PVD TiN is shown. (b) Device structure of PVD Ti/PVD TiN/HfO_2/Ru/ALD TiN/PVD TiN (c) Device structure of PVD Ti/PVD TiN/HfO_2/TaN/PVD TiN

Various MIM structure of the RRAM fabricated at TEL contains different layers fabricated with different techniques. Three different structures were fabricated for comparison purposes with oxygen plasma treated dielectric and different top metal electrode. Figure 3.1(a) (TiN-Device) shows structure for 5nm PVD TiN deposited on the top of 6nm oxide layer which is reactive to oxygen as discussed in previous chapter. These structures are discussed later for comparison to Ru top metal with plasma treated HfO_2 switching layer.

Figure 3.1(b) (Ru-Device) has structure with 5nm Ru deposited on top of 6nm oxygen plasma treated dielectric layer. 5nm ALD TiN and 50nm PVD TiN is deposited on top of Ru metal. As discussed before, Ru metal forms an interfacial layer at the interface. TiN acts as padding metal and oxygen scavenging metal electrode which helps in controlled formation of CF and reduction in power requirement for the RRAM. As shown in figure similar bottom electrode is deposited in all the three structure with 10nm PVD Ti and 50nm PVD TiN deposited in top if Si substrate. Top electrode and dielectric layer are etched for experimental research purposes.

Figure 3.1(c) (TaN-Device) shows structure for 5nm TaN deposited on the top of 6nm oxide layer that acts as oxygen scavenging layer by reacting with free oxygen ions in the oxide/metal interface and reduces the power requirement. 50nm PVD TiN is deposited on top of TaN as an extra oxygen reactive layer and a padding layer. Top electrode and dielectric layer are also etched for this device.

3.3 Electrical Characterization of The Devices

Figure 3.2 Picture of Keysight B1500 semiconductor device parameter analyzer**.**

Figure 3.3 The remote-sense and switch unit is shown which is connecter to the B1500A and probe station.

A Keysight B1500 semiconductor device parameter analyzer was used to perform the electrical characterization shown in figure 3.2. It is the next-generation semiconductor parameter analyzer that has the measurement capabilities required to test the reliability of advanced CMOS LSI (large scale integration) circuits. Moreover, the resident EasyEXPERT control software of the B1500A comes with ready-to-use measurement libraries covering all of the typical reliability tests for CMOS devices.

The B1500A Semiconductor Device Analyzer is primarily used in our work to take on the I-V characteristics of RRAM devices. The B1500A needs to be paired with a probe in time to capture RRAM measurement. By inserting the wafer in the grounded chuck, the probe system is used to take the RRAM wafer and to allow improved microscopic observation. As can be seen in Fig 3.3, the relation between B1500A and the prober system is accomplished via an accessory called RSU (the remote-sense and switch unit). We should also use two probes in our experiment. One probe is attached to the surface of the top electrode of the RRAM unit and the other is connected to the grounded probe station chuck, which is a wafer placement platform that needs to be tested in the

microscopic method. The Keysight EasyEXPERT software, which exists on the PC-based B1500A, is a powerful Microsoft Windows parametric application program.

Combined with an elegant graphical user interface, EasyEXPERT offers an easy and efficient measurement and analysis environment. By using a convenient graphical user interface, different parameters can be configured. By setting the double I-V sweep curve, the I-V characteristics of ReRAM devices can be measured. The method of measurement can be switched between a single cycle and a repetitive cycle. Often after continuous application of the reset phase, the higher R_{off} value is achieved, which can be accomplished independently by running the reset cycle to allow a full conductive filament split. The measured noise levels of B1500A are ≤ ±10pA at 4V, however the light source was turned off for noise reduction caused due to photons.

3.4 Principle of IV Characteristics

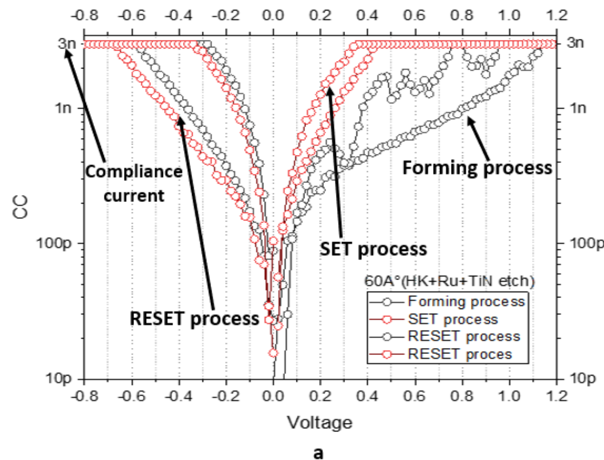

Figure 3.4 The graph shows the forming process, SET-RESET process and the compliance current in the I-V characteristic of a general oxide-based RRAM.

A typical current-voltage (I-V) characteristic of a RRAM cell in log-scale is shown in the figure 3.3 with initial current sweep and hysteresis behavior which shows the change in

resistance and therefore able to write and erase memory. The figure 3.3 shows the bipolar forming process for a typical RRAM cell. However, the forming voltage may differ with device to device for same metal electrode and it will also differ for different structure of the RRAM devices. As discussed in chapter 2, the forming process involves the initial CF formation in the switching layer and changing the device from HRS to LRS. RRAM with oxygen vacancies migration (which are studied in this thesis) involves formation of oxygen ions and reaction with top metal electrode to form an interfacial layer and leaving behind oxygen vacancies that cluster around and form a conductive path for electrons to migrate.

As shown in the figure 3.3 forming voltage is typically higher than the SET voltage as higher voltage is require for soft dielectric breakdown. To find the correct forming voltage, the compliance current (CC) was gradually increased from lower current to higher current till the soft dielectric breakdown occurs within the switching dielectric and a CF is formed. Also, gradual increase of CC is required for soft dielectric breakdown, jumping to higher voltage can lead to hard dielectric breakdown and a non-reversible CF is formed and ability of RRAM to switch from HRS to LRS and vice a versa is lost. The increase of CC for finding the forming voltage was started from 1nA and 3V. For the Ru devices the forming voltage was typically around 1V with 3-15nA CC, whereas for TiN it was 500mV with 500nA-1.5uA CC and 1.5V with 1.5-2uA CC for TaN devices. After the CF is formed, the RESET process ruptures the filament and HRS is obtained. For device to switch to LRS again the SET process must be performed. The CC current can be reduced to lower the power until LRS and HRS are

distinguishable, also it can be increased above the forming process current for a more distinguishable LRS and HRS.

3.5 Summary

Experimental details of the thesis are explored in this chapter, the probing techniques, and structures of the devices is discussed in detail. Deposition techniques used for fabrication of the devices are discussed in brief, also the details for reading the I-V characteristics are explained in section 3.4 with pointing out the forming and the SET-RESET process.

CHAPTER 4

RESULTS OF TREATED DEVICES TO ENHANCE OXYGEN VACANCIES

I-V characteristics of the devices are studied in this chapter, SET-RESET I-V graphs of the devices that are to be compared in next chapter are explained in detail. As discussed before oxygen vacancies are responsible for the CF formation, and metal/oxide interface properties of the top metal plays major role in power reduction, stability and the endurance of the RRAM devices.

4.1 TiN Devices

TiN is extensively used in CMOS technology as a gate metal. Therefore, it is more suitable for RRAM devices. Figure 4.1 shows logarithmic I-V characteristics of TiN devices with different CC. The cross-section of the device is shown in figure 3.1(a). Forming process was carried out by gradually increasing the CC from 3nA to 500nA and 800nA, at which forming happened for the three devices shown in the figure 4.1.

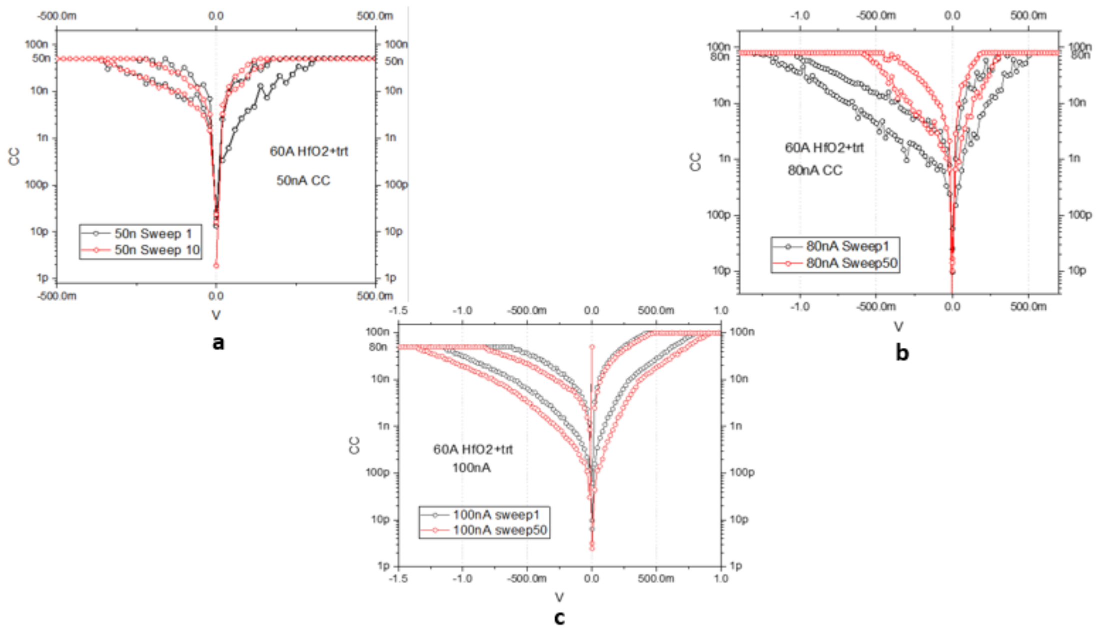

Figure 4.1 I-V characteristics of the devices with TiN as top electrode is shown. (a) set-reset sweeps of 1st and 10th cycle are shown for CC of 50nA(b) 1st and 50th cycle set-reset sweeps are shown for CC of 80nA (c) 1st and 50th cycle set-reset sweeps are shown for CC of 100nA.

After the forming process, the SET voltage was reduced with well enough separated LRS and HRS. It is known that once the filament is ruptured after the RESET process a gap between the partially existing CF and top metal contributes to HRS. figure 4.1(a) shows I-V characteristic at 50nA CC. It can be seen that the initial forming voltage is higher than the SET voltage of the subsequent cycles at this CC. However, the device was able to switch for 10 cycles before a permanent non-reversible CF was formed. figure 4.1(b) shows device with higher CC at 80nA was set and 50+ cycles of SET and RESET process were carried out. Due to smaller RESET CC more clustering of oxygen vacancies formed near the top electrode and the gap between the top electrode and ruptured filament reduced to a point where only few oxygen ions were able to recombine with oxygen vacancies in HRS state. Therefore, the difference between the LRS and HRS

was indistinguishable. Higher CC of 100nA was subsequently used for the device shown in figure 4.1(c), where a more distinguishable LRS and HRS was observed even after more than 50 cycles of SET and RESET process. The forming voltage has increased slightly as the compliance was increased.

4.2 Ru Devices

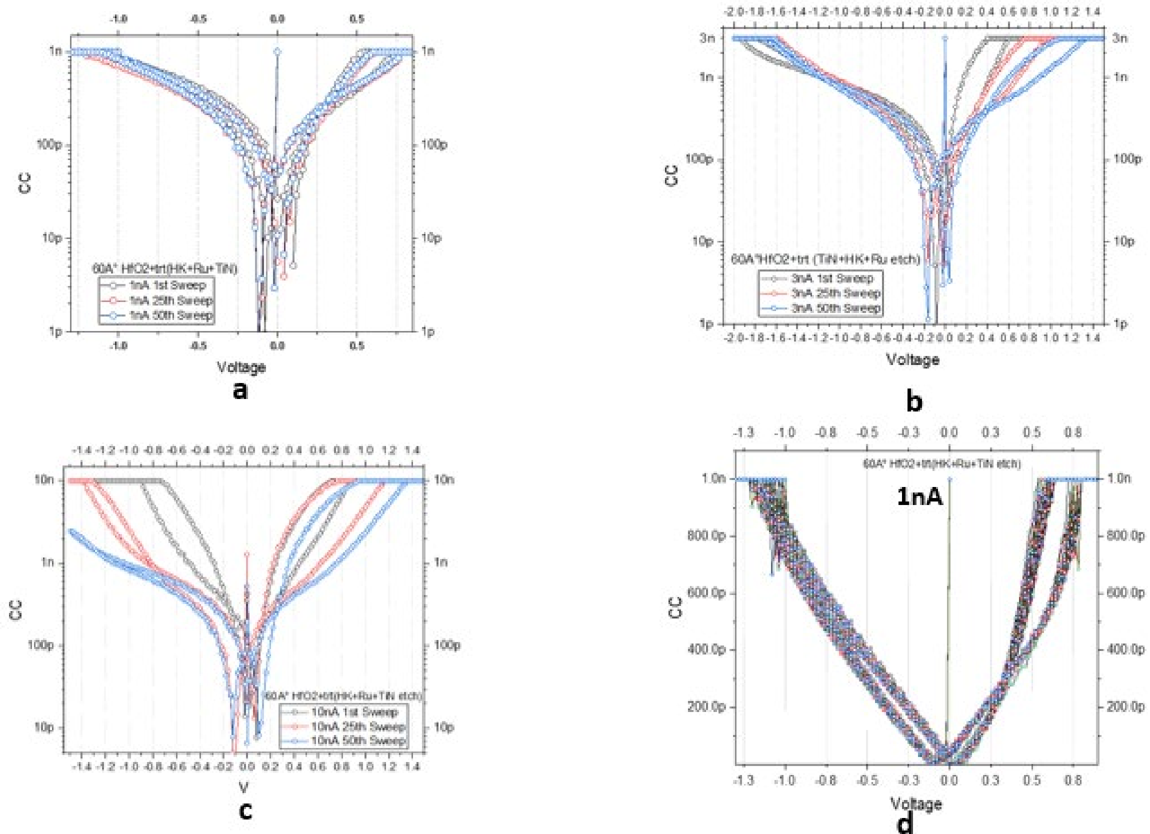

Figure 4.2 I-V characteristics of the devices with Ru as top electrode is shown. (a) Three (1st, 25th and 50th) set-reset sweeps are shown with CC of 1nA, (b) Three (1st, 25th and 50th) set-reset sweeps are shown with CC of 3nA (c) Three (1st, 25th and 50th) set-reset sweeps are shown with CC of 10nA (d) Linear scale of all 50 cycles of 1nA CC is shown in this plot.

I-V characteristics of devices with Ru as top electrode is shown in the figure 4.2. The cross-section of this device is shown in Fig. 3.1(b). The switching CC current was reduced significantly for this device. The device has, therefore, demonstrated a very low power consuming characteristic mainly due to plasma treatment on HfO_2 layer and interfacing oxide formation of Ru with oxygen ions and oxygen scavenging TiN layer as discussed in chapter 2. The forming voltage was found to be 1V at 10nA CC. However, some devices showed lower forming voltage at 1nA CC. Figure 4.2(a) shows three cycles of SET and RESET from more than 50 cycles with 1nA CC, which was the lowest CC achieved for switching for all the devices investigated in this thesis. Figure 4.2(d) shows the linear representation of 50 cycles of the switching process, tighter formation of SET and RESET cycles is observed which is an important property of memory storage devices. Cycles with higher CC was carried out for comparison purposes, Fig. 4.2(b) and figure 4.2(c) shows I-V graphs with 3nA CC and 10nA respectively. More than 50 cycles were carried out for each of the CC. A trend of an increase in SET voltage and RESET voltage was observed. Since some of the devices seize to perform after several cycles different CC was studied but only graphs of three CCs are shown here. Also, more than 200 cycles were performed on a single device that demonstrate higher endurance rate. Additionally, switching at multiple compliance currents in a single device represents multi-level resistance (or conductance) states.

4.3 TaN Devices

Devices with TaN as a top electrode metal, TaN Devices (Fig. 3.1(c)) , were studied to investigate the switching power requirements. As discussed earlier in chapter 2 TaN

devices are less reactive towards oxygen than Ti and TiN which leads to increase in CC and forming voltage.

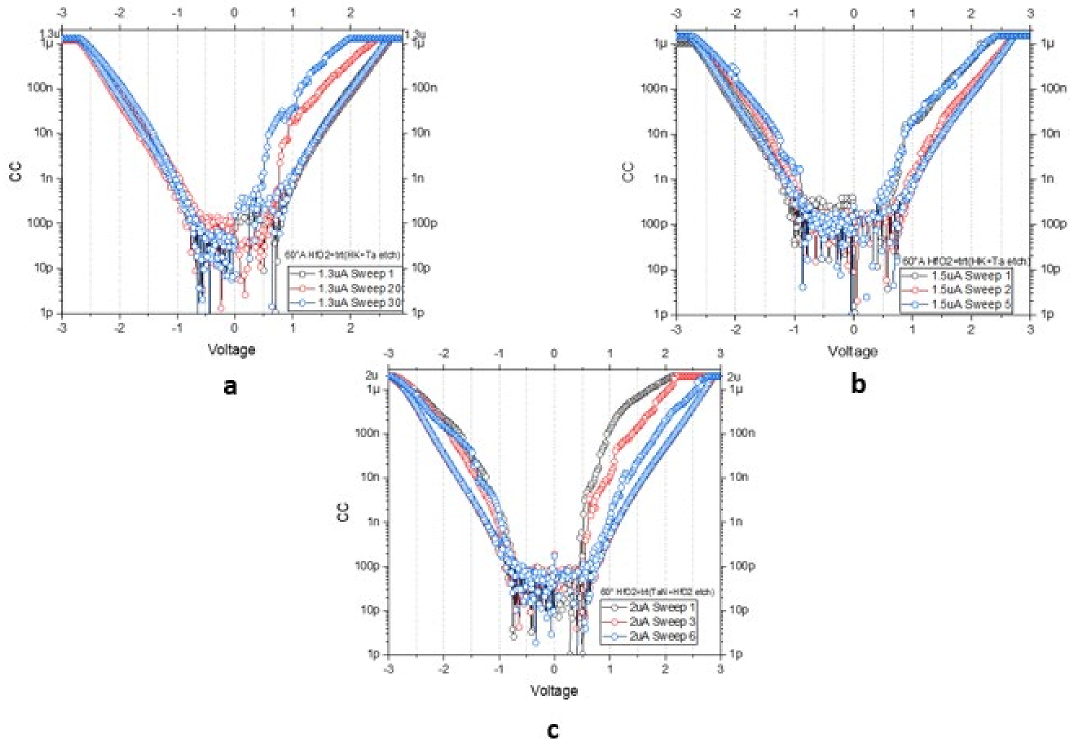

Figure 4.3 I-V characteristics of the devices with TaN as top electrode is shown. (a) Three (1st, 20th and 30th) set-reset sweeps are shown with CC of 1.3uA (b) Three (1st, 2nd and 5th) set-reset sweeps are shown with CC of 1.5uA. (c)Three (1st, 3rd and 6th) set-reset sweeps are shown with CC of 2uA.

As shown in the figure 4.3, higher CC of 1 μA was required for device to form CF and able to toggle between LRS and HRS states. Figure 4.3(a) shows three cycles with a CC of 1.3uA where the devices was less stable and the LRS and HRS states were indistinguishable. However, the device worked up to 50 switching cycles that were performed on the device. Higher CC with 1.5uA and 2uA are shown in figure 4.3(b) and figure 4.3(c) respectively. Devices formed a permanent non-reversible CF after switching

for few cycles, which shows less stability and endurance rate than previous studied devices.

4.4 Summary

In this chapter I-V characteristics of RRAM devices with TiN, Ru and TaN as top electrode were described with details on the forming voltage, set voltage and the CC. Device with Ru and TiN has shown good characteristics with power reduction due to it reactivity and scavenging capabilities towards oxygen ions at the metal/dielectric interface. Ru as a top metal showed the lowest switching power. However, devices with TaN showed higher switching power requirement than other two RRAM devices.

CHAPTER 5

COMPARISION OF DIFFERENT METALS

Comparison of switching characteristics of the devices were mentioned in chapter 4. This chapter the resistance distribution of these devices as a function of compliance current is evaluated and compared. As seen previously, different top metal electrode tends to show different characteristics with oxygen defects rich HfO_2 dielectric layer. Comparison of the results helps to decide the device configuration needed for multi-level resistance state.

5.1 Comparison Between Ru and TaN, TiN Devices

Assuming the initial oxygen vacancy distribution in the plasma treated HfO_2 layer is identical, the switching characteristics described in chapter 4 demonstrate a significant variation. The top electrode material is, therefore, responsible for the observed variation. Ru has one electron in its outer most orbit while Ta and Ti has two electrons. As studied in chapter 2, Schottky barrier height can be changed by top electrode if the oxygen is weakly bonded in the dielectric layer [53]. While the oxygen scavenging properties of TaN and TiN are similar TiN has higher reactivity towards the free oxygen ion. According to other studies, the barrier height of TaN/HfO_2 is 4.6eV [54], barrier height of TiN/HfO_2 is 3.7ev [49]. The difference in the work function and Schottky barrier height can be accountable for the variation in characteristics.

When Ru is placed in contact with HfO_2 (Ru/HfO_2 interface) it has higher work function compare to metallic Ru. The oxidation process at the interface increases the work function. The studies have suggested a work function of Ru at Ru/HfO_2 interface is

4.5eV [37]. Furthermore, the plasma treatment of the HfO_2 layer does incorporates chemical species at the metal/dielectric interface and causes changes in the electrostatic potential and affects the work function of the top metal electrode.

The change in work function, interface barrier and application of different compliance current have different effects on the CF formation. Multi-level storage capabilities can be seen in the IV characteristics (Fig. 4.2) with CC of 3nA and 10nA respectively whereas for CC 1nA a tighter trend is observed, also this difference in trends can suggest possibility of a single CF with larger diameter or multiple CF formation with different diameters [53][31].

5.2 Switching Characteristics

As discussed before chapter 1 and 2, the switching mechanism of the RRAM, involves the forming process and the SET-RESET process. However, the switching characteristics of the devices involves different chemical reactions at the interface layers, which affects the physical properties of the formed oxide layer such as activation energy and diffusion barrier. The free ions formed at the interface, reacts with TiN, TaN and Ru to form an oxide layer with different concentration. Also, during the fabrication process of deposition, more oxygen vacancies are formed by oxygen migration into the metal electrodes [55].

5.3 Resistance Distribution

5.3.1 Resistance Distribution in Ru Devices

Figure 5.1(a) shows the cumulative distribution frequency vs resistance plots of the Ru top electrode devices, the x-axis is the resistance values of SET switching cycle and the y-axis is the frequency of distribution. R_{high} represents the resistance at HRS, while R_{low} represents the resistance at LRS. Figure 5.1(b) shows the resistance variation across the 50 cycles for both 1 nA and 3 nA compliance current. The resistance distribution was plotted to see the spread in the resistance over the 50 consecutive switching cycles, to deduce if the device can be used for in-memory computing such as neuromorphic computing (as a synapse) and multilevel storage cell (MLC).

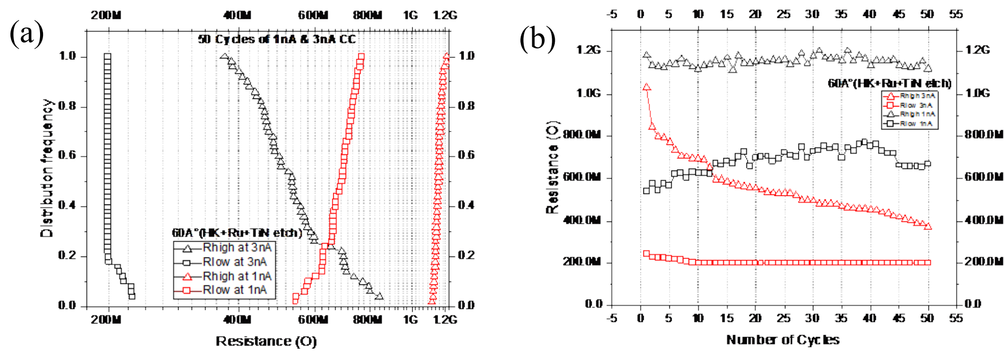

Figure 5.1 Cumulative Resistance distribution of the devices with Ru as top electrode is shown. (a) Cumulative distribution of resistance of 50 cycles at 0.6V with 3nA CC and at 0.54V with 1nA CC, (b) Resistance variation across the 50 cycles for both the compliance currents.

The resistance distribution of 50 SET-RESET cycles is shown for Ru Devices at 1nA and 3nA CC at 0.54V and 0.6V respectively. Similar trend was observed for 5nA CC. The resistance distribution for HRS is from 1.1GΩ to 1.2GΩ for 1 nA CC whereas

the resistance spread for 3 nA CC in HRS is from 400 to 1GΩ. The LRS distribution is with the range of 700 MΩ for 1 nA CC whereas the resistance spread for 3 nA CC is around 200 MΩ. The resistance variation for both the cases remains uniform except the R_{high} for 3 nA CC. As shown in Fig. 5.2 because of CF characteristics thickness this variation is expected. At lower compliance current the filament is thinner or only a few established conducting channels across the electrodes. This leads to higher R_{low} as compared to R_{low} for higher CC. The reverse is true for R_{high} as the ruptured CF is significant in case of low CC as compared to high CC. This characteristic demonstrates that by adjusting the resistance according to the requirement can implement MLC capability.

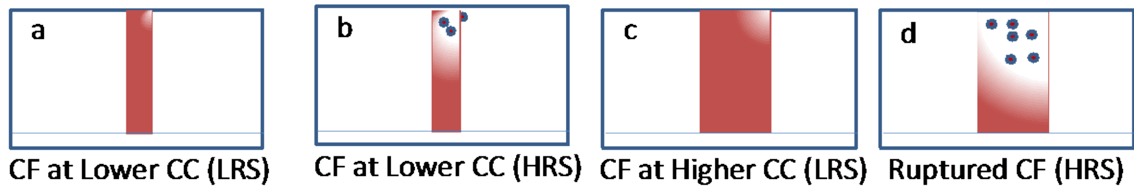

Figure 5.2 Conducting Filament formation as a function of compliance current. (a) at lower compliance current (LRS), (b) Ruptured CF at lower compliance current (HRS), (c) at a higher compliance current (LRS) and (c) ruptured CF at higher compliance current (HRS).

5.3.2 Resistance Distribution in TiN Devices

When TiN is a top electrode metal the behavior is quite different because of its reactivity with oxygen ions and scavenging oxygen from the switching dielectric.

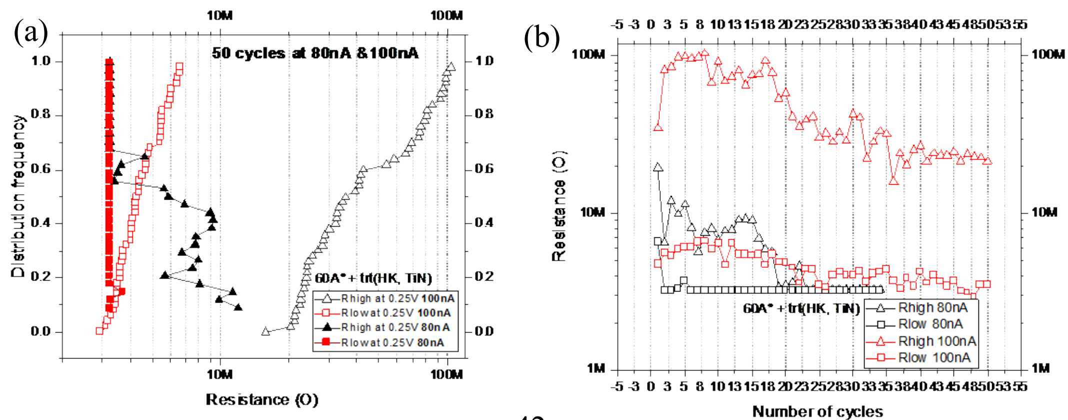

Figure 5.3 Cumulative Resistance distribution of the devices with TiN as top electrode is shown. Resistance distribution of 50 cycles at 0.25V with 100nA CC.

RESET cycles at 80 nA and 100 nA of CC and 0.25V. The resistance spread of HRS is from 20MΩ to 100MΩ, which shows limited MLC capabilities as discussed earlier. The resistance variation across the cycles in Figure 5.3(b) shows a decrease in resistance value as cycle number is increased except for R_{low} at 80 nA CC. As mentioned earlier the TiN RRAM devices showed the resistance values are much smaller than Ru devices. It is because after the metal deposition excess oxygen ions were scavenged to the TiN/HfO_2 interface. The oxygen reaction led to the excess defects in HfO_2 layer in addition to the defects induced due to oxygen plasma treatment. This brings down the SET voltage and thereby reduces the resistance values from LRS and HRS.

5.3.3 Resistance Distribution in TaN Devices

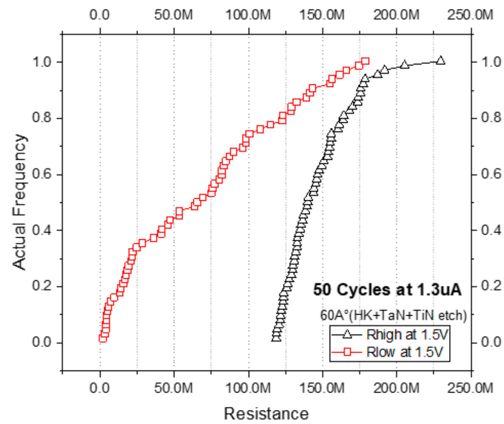

Figure 5.4 Cumulative Resistance distribution of the devices with TaN as top electrode is shown. Resistance distribution of 50 cycles at 1.25V with 1.3uA CC.

Figure 5.4 shows the cumulative resistance distribution of TaN device for 50 SET-RESET cycles at 1.3uACC at 1.5V. The resistance distribution of TaN has a spread for both HRS and LRS, this shows that set voltage is not very controlled. As mentioned earlier the SET voltage increases as the cycles proceed. TaN has similar oxygen scavenging properties as TiN, but different work function and Schottky barrier, that can be a possible explanation for less endurance and less controllability of CF.

5.4 Summary

Comparison of the three top metal electrodes was performed in this chapter by comparing the resistance plots and comparing the results from Ch. 4. To summarize, Ru devices showed distinct resistance distribution by alteration of CCs from 1nA to higher CCs. All three devices showed MLC capabilities and compatible with learning devices, such as an

electronic synapse. Conclusion can be made that engineering the top electrode and oxygen plasma treatment on the dielectric layer can reduce the switching power.

CHAPTER 6

CONCLUSION AND FUTURE WORKS

The formation of CF in HfO_2 lattice, with effects of top electrode selection in RRAM is studied in this thesis. Detailed working of transition metal oxide RRAM devices with oxygen migration mechanism is been investigated. Oxygen defects introduced in HfO_2 by plasma exposure plays a major role in formation of CF, we also studied the nature of the oxygen vacancies that form the CF and accounts for reaction with top metal electrode. The knocked-out oxygen ions react to bring down the forming and the set voltage and the oxygen vacancies formed can acts as charge trapping centers.

The advantages of HfO_x over HfO_2, described in Ch. 2, the defect formation energy of stoichiometric hafnium oxide is higher than non-stoichiometric hafnium oxide which accounts for higher diffusion barrier therefore a reactive top metal is introduced to lower the diffusion barrier and formation of oxygen vacancies that are needed for CF formation. Top metal electrodes are studied in detail, their physical and chemical properties are considered for the interfacial reaction between metal and oxide layer. Also, plasma treatment on the HfO_2 is studied in this work for the extra injection of defects that favored in reducing switching power for CF formation and rupturing of the CF. Effect of Schottky barrier height is also studied in brief for explaining the switching mechanism involving different top metal electrodes.

The details of the experimental procedures and device fabrication was outlined in chapter 3. Explanation of the importance of compliance current to limit the breakdown and formation of CF is shown with graphical explanation for better understanding. Set and reset process are also shown in the graph to better understand the results discussed in

chapter 4. After understanding of the background, the results of the study conducted in this thesis are presented in the chapter 4. Graphs with different CC on the devices with different top metal electrode is demonstrated. The obtained results are discussed in the following chapter, with comparison of different top metal electrodes and the switching mechanisms. Finally, the resistance distribution of the obtained I-V characteristics of different devices are discussed.

In summary, the thesis studies the role of top metal electrode and dielectric layer in power reduction, which is a deciding factor in today's semiconductor industry. However, more research is needed towards this direction to produce RRAM devices which can be brough to production market. More research on the physical and chemical properties of the layers needs to be conducted, with development of a perfect switching model for RRAM that preciously explains all the responsible parameters and constrains.

6.1 Future Work

Use of Ru, TiN and TaN as the bottom metal needs to be investigated to further understand the effectiveness of these electrode metals to enhance the performance and power requirements of RRAM devices.

REFERENCES

[1] *Silicon, Interconnect, Packaging and Test Challenges from a Foundry Viewpoint*. June 2015, www.swtest.org/swtw_library/2015proc/PDF/SWTW2015_Keynote_McCann_GlobalFoundries.pdf.

[2] JS. Meena, SM. Sze, et al. "Resistive Random Access Memory (RRAM): an Overview of Materials, Switching Mechanism, Performance, Multilevel Cell (Mlc) Storage, Modeling, and Applications." *Nanoscale Research Letters*, SpringerOpen, 1 Jan. 1970, nanoscalereslett.springeropen.com/articles/10.1186/s11671-020-03299-9.

[3] A. Levisse; B. Giraud; J.-P. Noel; M. Moreau; J.-M. Portal. "RRAM Crossbar Arrays for Storage Class Memory Applications." *RRAM Crossbar Arrays for Storage Class Memory Applications: Throughput and Density Considerations - IEEE Conference Publication*, 2018, ieeexplore.ieee.org/document/8681470.

[4] T. W. Hickmott, BLow-frequency negative resistance in thin anodic oxide films,[J. Appl. Phys., vol. 33, 2669, 1962.

[5] J. F. Gibbons and W. E. Beadle, BSwitching properties of thin NIO films,[Solid-State Electron., vol. 7, no. 11, pp. 785–790, 1964.

[6] G. Dearnale, A. M. Stoneham, and D. V. Morgan, BElectrical phenomena in amorphous oxide films,[Rep. Progr. Phys., vol. 33, 1129, 1970.

[7] Hong, L. (2018). Oxide-based RRAM materials for neuromorphic computing. *Journal of Materials Science*, *53*(12), 8720–8746. https://doi.org/10.1007/s10853-018-2134-6

[8] Wong, L. (2012). Metal–Oxide RRAM. *Proceedings of the IEEE*, *100*(6), 1951–1970. https://doi.org/10.1109/jproc.2012.2190369

[9] Zhu, Linggang, et al. "An Overview of Materials Issues in Resistive Random Access Memory." *Journal of Materiomics*, Elsevier, 30 July 2015, www.sciencedirect.com/science/article/pii/S2352847815000568.

[10] Gao, Shuang, et al. "Implementation of Complete Boolean Logic Functions in Single Complementary Resistive Switch." *Nature News*, Nature Publishing Group, 21 Oct. 2015, www.nature.com/articles/srep15467.

[11] Eshita, W. (2014). Development of ferroelectric RAM (FRAM) for mass production. *2014 Joint IEEE International Symposium on the Applications of Ferroelectric, International Workshop on Acoustic Transduction Materials and Devices & Workshop on Piezoresponse Force Microscopy*, 1–3. https://doi.org/10.1109/ISAF.2014.6922970

[12] A: W. I. Kinney, W. Shepherd, W. Miller, J. Evans, and R. Womack, “A non-volatile memory cell based on ferroelectric storage capacitors,” in Proc. Int. Electron DevicesMeet. Tech. Dig., 1987, pp. 850–851.

[13] Thomas, J. (2014). Perpendicular spin transfer torque magnetic random access memories with high spin torque efficiency and thermal stability for embedded applications (invited). Journal of Applied Physics, 115(17), 172615–. https://doi.org/10.1063/1.4870917

[14] Peng, S., Zhang, Y., Wang, M., Zhang, Y., & Zhao, W. (2014, December 15). Magnetic Tunnel Junctions for Spintronics: Principles and Applications. Retrieved December 07, 2020, from https://onlinelibrary.wiley.com/doi/10.1002/047134608X.W8231

[15] Hamsa, S., Thangadurai, N. & Ananth, A.G. Low power device design application by magnetic tunnel junctions in Magnetoresistive Random Access Memory (MRAM). *SN Appl. Sci.* 1, 828 (2019). https://doi.org/10.1007/s42452-019-0826-4

[16] Song, D. (2020). Impact of Process Variability on Write Error Rate and Read Disturbance in STT-MRAM Devices. IEEE Transactions on Magnetics, 56(12), 1–11. https://doi.org/10.1109/TMAG.2020.3028045

[17] H. -. P. Wong et al., "Phase Change Memory," in Proceedings of the IEEE, vol. 98, no. 12, pp. 2201-2227, Dec. 2010, doi: 10.1109/JPROC.2010.2070050.

[18] Le Gallo, S. (2020). An overview of phase-change memory device physics. Journal of Physics. D, Applied Physics, 53(21), 213002–. https://doi.org/10.1088/1361-6463/ab7794

[19] Yu, W. (2011). Compact Modeling of Conducting-Bridge Random-Access Memory (CBRAM). IEEE Transactions on Electron Devices, 58(5), 1352–1360. https://doi.org/10.1109/TED.2011.2116120

[20] Kwon, K., Kim, D., Kim, H., Jin, S., Woo, D., Park, S., & Park, J. (2020, May 04). An electroforming-free mechanism for Cu2O solid-electrolyte-based conductive-bridge random access memory (CBRAM). Retrieved December 07, 2020, from https://doi.org/10.1039/D0TC01325K

[21] Yu, W. (2010). A Phenomenological Model for the Reset Mechanism of Metal Oxide RRAM. IEEE Electron Device Letters, 31(12), 1455–1457. https://doi.org/10.1109/LED.2010.2078794

[22] Kumar, A. (2017). Metal oxide resistive switching memory: Materials, properties and switching mechanisms. Ceramics International, 43, S547–S556. https://doi.org/10.1016/j.ceramint.2017.05.289

[23] Feng PAN, h. (2010). Nonvolatile resistive switching memories-characteristics,mechanisms and challenges. Progress in Natural Science, 20(1), 1–15. https://doi.org/10.1016/s1002-0071(12)60001-x

[24] Zahoor, A. (2020). Resistive Random Access Memory (RRAM): an Overview of Materials, Switching Mechanism, Performance, Multilevel Cell (mlc) Storage, Modeling, and Applications. Nanoscale Research Letters, 15(1), 90–90. https://doi.org/10.1186/s11671-020-03299-9

[25] Garbin, V. (2015). HfO2-Based OxRAM Devices as Synapses for Convolutional Neural Networks. IEEE Transactions on Electron Devices, 62(8), 2494–2501. https://doi.org/10.1109/ted.2015.2440102

[26] Gilmer, B. (2011). Effects of RRAM Stack Configuration on Forming Voltage and Current Overshoot. 2011 3rd IEEE International Memory Workshop (IMW), 1–4. https://doi.org/10.1109/IMW.2011.5873225

[27] Jain, H. (2019). Multilevel Resistive Switching in Hf-Based RRAM. ECS Transactions, 89(3), 39–44. https://doi.org/10.1149/08903.0039ecst

[28] Jain, H. (2019). Multilevel Resistive Switching in Hf-Based RRAM. ECS Transactions, 89(3), 39–44. https://doi.org/10.1149/08903.0039ecst

[29] Ambrogio, B. (2016). Neuromorphic Learning and Recognition With One-Transistor-One-Resistor Synapses and Bistable Metal Oxide RRAM. IEEE Transactions on Electron Devices, 63(4), 1508–1515. https://doi.org/10.1109/ted.2016.2526647

[30] Chung, C. (2020). A Study of the Relationship Between Endurance and Retention Reliability for a HfO_x-Based Resistive Switching Memory. IEEE Transactions on Device and Materials Reliability, 20(3), 541–547. https://doi.org/10.1109/TDMR.2020.3007172

[31] Misra, Z. (2020). Dielectrics and Metal Stack Engineering for Multilevel Resistive Random-Access Memory. ECS Journal of Solid State Science and Technology, 9(5), 53004–. https://doi.org/10.1149/2162-8777/ab9dc5

[32] Fang, Y. (2018). Improvement of HfOx-Based RRAM Device Variation by Inserting ALD TiN Buffer Layer. IEEE Electron Device Letters, 39(6), 819–822. https://doi.org/10.1109/LED.2018.2831698

[33] Xue, B. (2013). Grain boundary composition and conduction in HfO2: An ab initio study. Applied Physics Letters, 102(20), 201908–. https://doi.org/10.1063/1.4807666

[34] B. Traoré et al., "Impact of electrode nature on the filament formation and variability in HfO2 RRAM," 2014 IEEE International Reliability Physics Symposium, Waikoloa, HI, 2014, pp. 5E.2.1-5E.2.5, doi: 10.1109/IRPS.2014.6860676.

[35] Lee, C. (2008). Low power and high speed bipolar switching with a thin reactive Ti buffer layer in robust HfO2 based RRAM. 2008 IEEE International Electron Devices Meeting, 1–4. https://doi.org/10.1109/IEDM.2008.4796677

[36] Al-Mamun, M. (2019, November 11). Impact of Inert-electrode on the Performance and Electro-thermal Reliability of ReRAM Memory Array. Retrieved December 07, 2020, from https://vtechworks.lib.vt.edu/handle/10919/95489

[37] Nabatame, S. (2006). The effect of oxygen in Ru gate electrode on effective work function of Ru/HfO2 stack structure. Materials Science in Semiconductor Processing, 9(6), 975–979. https://doi.org/10.1016/j.mssp.2006.10.013

[38] Pantisano, S. (2006). Ruthenium gate electrodes on SiO2 and HfO2: Sensitivity to hydrogen and oxygen ambients. Applied Physics Letters, 88(24), 243514–. https://doi.org/10.1063/1.2212288

[39] He, W. (2019). Atomic Layer-Deposited HfAlOx-Based RRAM with Low Operating Voltage for Computing In-Memory Applications. Nanoscale Research Letters, 14(1), 51–51. https://doi.org/10.1186/s11671-019-2875-4

[40] Li, T. (2020). Initial states and analog switching behaviors of two major tantalum oxide resistive memories. Japanese Journal of Applied Physics, 59(4), 44004–. https://doi.org/10.35848/1347-4065/ab8022

[41] Ismail, A. (2015). Role of tantalum nitride as active top electrode in electroforming -free bipolar resistive switching behavior of cerium oxide-based memory cells. Thin Solid Films, 583, 95–101. https://doi.org/10.1016/j.tsf.2015.03.059

[42] Sun, L. (2019). The Resistive Switching Characteristics of TiN/HfO2/Ag RRAM Devices with Bidirectional Current Compliance. Journal of Electronic Materials, 48(5), 2992–2999. https://doi.org/10.1007/s11664-019-07069-x

[43] Fang, Y. (2018). Improvement of HfOx-Based RRAM Device Variation by Inserting ALD TiN Buffer Layer. IEEE Electron Device Letters, 39(6), 819–822. https://doi.org/10.1109/LED.2018.2831698

[44] Misra, Z. (2020). Dielectrics and Metal Stack Engineering for Multilevel Resistive Random-Access Memory. ECS Journal of Solid State Science and Technology, 9(5), 53004–. https://doi.org/10.1149/2162-8777/ab9dc5

[45] Traoré, B. (2015). Investigation of HfO2-based resistive RAM cells by electrical characterization and atomistic simulations.

[46] Chand, H. (2015). Suppression of endurance degradation by utilizing oxygen plasma treatment in
HfO2 resistive switching memory. Applied Physics Letters, 106(15), 153502–. https://doi.org/10.1063/1.4918679

[47] Zhirnov, V., & Cavin, R. (2015). *Microsystems for bioelectronics : scaling and performance limits* (Second edition.). Elsevier.

[48] Pantisano, A. (2011). Towards barrier height modulation in HfO2/TiN by oxygen scavenging – Dielectric defects or metal induced gap states? Microelectronic Engineering, 88(7), 1251–1254. https://doi.org/10.1016/j.mee.2011.03.057

[49] Pandey, S. (2013). Role of point defects and HfO2/TiN interface stoichiometry on effective work function modulation in ultra-scaled complementary metal–oxide–semiconductor devices. Journal of Applied Physics, 114(3), 34505–. https://doi.org/10.1063/1.4816090

[50] Pan, Ding. "High-Temperature Conduction Behaviors of HfO2/TaN-Based Metal-Insulator-Metal Capacitors." Journal of applied physics 102, no. 7 (October 2007): 73706–.

[51] S. Chew et al., "Ultralow resistive wrap around contact to scaled FinFET devices by using ALD-Ti contact metal," 2017 IEEE International Interconnect Technology Conference (IITC), Hsinchu, 2017, pp. 1-3, doi: 10.1109/IITC-AMC.2017.7968969.

[52] Bhuyian, P. (2015). Impact of cyclic plasma treatment on oxygen vacancy defects in TiN/HfZrO/SiON/Si gate stacks. Applied Physics Letters, 106(19), 193508–. https://doi.org/10.1063/1.4921307

[53] Slesazeck, M. (2019). Nanoscale resistive switching memory devices: a review. Nanotechnology, 30(35), 352003–. https://doi.org/10.1088/1361-6528/ab2084

[54] Sugimoto, K. (2008). Dependences of effective work functions of TaN on HfO2 and SiO2 on post-metallization anneal. Thin Solid Films, 517(1), 204–206. https://doi.org/10.1016/j.tsf.2008.08.058

[55] Traore, B. (2018). HfO2/Ti Interface Mediated Conductive Filament Formation in RRAM: An Ab Initio Study. IEEE Transactions on Electron Devices, 65(2), 507–513. https://doi.org/10.1109/TED.2017.2785352